Pergamon

Int. J. Mech. Sci. Vol. 38, No. 2, pp. 141–155, 1996

0020–7403/96 $9.50 + 0.00

0020-7403(95)00045-3

THE MACHINING OF SINTERED BRONZE

N. A. FLECK, K. J. KANG† and J. A. WILLIAMS

Cambridge University Engineering Department, Trumpington Street, Cambridge, CB2 1PZ, U.K. and
†Department of Mechanical Engineering, Chonnam National University, Kwangju 500-757 Republic of Korea

(*Received* 1 *August* 1994; *and in revised form* 16 *February* 1995)

Abstract—Orthogonal machining experiments have been conducted on specimens of sintered bronze. At low porosities and low depths of cut, a continuous chip is formed as a result of compaction and shear local to the tip of the tool. At higher porosities, and larger depths of cut, discontinuous chips form due to alternate compaction of the chip and brittle fracture. The transition occurs when the depth of cut is about 0.6 times the size of the plastic zone size associated with brittle fracture.

NOTATION

α cutting tool rake angle
d depth of cut
t specimen thickness
f specimen porosity, percentage
$v, \dot{v}$ cutting tool displacement and velocity
l crack length
r_p characteristic plane strain plastic zone size at onset of brittle fracture
K_{IC} material plane strain fracture toughness
σ_f material flow stress
σ_y material yield strength
λ wavelength of force fluctuations during discontinuous chip formation
F principal cutting force
T transverse cutting force
μ coefficient of friction

1. INTRODUCTION

Sintered metals are used increasingly for mass production of precision mechanical engineering components of complex shape. Although the compaction and sintering process is a net shape forming process a small degree of final machining or grinding may be necessary. There appears to be a paucity of information on the mechanics of machining of sintered materials.

Geophysical materials such as agglomerates are composed of elastic–brittle particles such as quartzes bonded by clays (which behave in a ductile plastic manner). As yet there is incomplete knowledge of the cutting process of such rocks during rock drilling. The machining process certainly involves compaction of the aggregate and dissipation by inter-particle friction and perhaps plasticity. Thus porous metals are useful model materials in order to throw light on the machining of rocks. (The rock problem is of course a more complex one, as fragmentation of the rock and pore fluid effects are also present).

In this paper orthogonal machining tests are reported for sintered bronze. We investigate the dependence of the cutting mechanism and cutting force upon the initial porosity of the bronze, the machining depth and the rake angle of the tool.

2. MANUFACTURE OF MATERIAL AND MACHINING RIG

Gas atomized spherical bronze powder (composition 11% Sn–0.4%P–rem. Cu) was pressureless sintered in a vacuum furnace for 1 h, followed by a slow furnace cool. The final porosity f of the 10 mm × 10 mm × 50 mm rectangular specimens was controlled at 11%, 23% and 33% by setting the sintering temperature at 850°C, 800°C and 750°C, respectively. A representative view of the as-sintered material is shown in Fig. 1: the micrograph was

taken using a scanning electron microscope (SEM). The bronze particles are of diameter 50 ± 10 μm.

The as-sintered material was found to be close to isotropic in properties; typical uniaxial stress–strain curves are shown in Fig. 2, for $f = 11\%$ and $f = 33\%$. When f is increased from 11% to 33% Young's modulus E drops from 80 GPa to 19 GPa and the tensile yield strength σ_y drops from 142 MPa to 34 MPa, as summarized in Table 1. No significant difference was observed between the compressive and the tensile yield strengths. The small necks between particles lead to a low tensile ductility and a low fracture toughness for sintered materials. For the porous bronze the tensile ductility decreased from 5% to 2% when f was increased from 11% to 33%. As compaction proceeds in a compression test, so the stress required to maintain continued deformation grows markedly as the material shows a high degree of strain hardening; Fig. 2 shows that using specimens with initial porosities of 11 and 33% the effective compressive strength had grown, at a strain of unity, to about 560 and 960 MPa respectively. The fracture toughness K_{IC} of the sintered specimens was measured using a 3-point bend rig: we found that K_{IC} decreased from 16 MPa$\sqrt{\text{m}}$ to 1.5 MPa$\sqrt{\text{m}}$ as the porosity f increased from 11% to 33%: these values are typical for sintered bronzes.

Machining rig

The specimens were machined using a specially designed machining rig mounted in a screw driven test machine, as shown in Fig. 3. The tool was contained within a guide-way to allow for movement by a displacement v in the direction of the cutting force F, see Fig. 3. Four hardened steel tools were made, as sketched in Fig. 3, such that the rake angle α was either 0° or 45°, and the flank face was relieved by 0° or 5°. Strain gauges on the tools were used in order to deduce the transverse force T, and the load cell of the test machine used to measure the cutting force F.

The tool was driven at a constant velocity of $\dot{v} = 0.003$ mm/s and the tool displacement was measured using a linear voltage displacement transducer (LVDT). No lubrication was employed. In order to examine the deformation state near the tip of the tool, several specimens were split along their mid-plane using a diamond metallographic cutter. A square grid of 0.2 mm spacing was scribed on one face at mid-plane, and the two halves of the specimen were then put together and gripped in the machining rig. At the end of the machining test, the mid-plane of the specimen was examined using optical and scanning electron microscopy.

3. RESULTS

Most tests were carried out using the 45° tool, without relief on the flank face; we start by considering the results of these tests. In all tests with the 45° tool (both with 5° relief of flank angle, and with no relief) the transverse force T was always negative in sign and less than 5% of the cutting force F in magnitude. A negative value for T implies that the tool is pushing the chip away from the parent material. Two types of response were observed: continuous chip formation, and discontinuous chip formation. We consider each type of cutting mechanism in turn.

3.1. *Continuous chip formation*

Continuous chip formation was associated with low values of porosity f and small depths of cut d. Typical results are shown in Fig. 4, where the nominal machining pressure F/td, i.e. cutting force per unit area of material removed, is plotted against tool displacement, v. The magnitude of the cutting pressure (and transverse pressure T/td) decreases with increasing porosity: this is expected as the yield strength decreases markedly with increasing porosity. For a constant value of depth of cut $d = 0.4$ mm, the deformation mode is continuous chip formation at porosities of $f = 11\%$ and 23%; at the highest porosity $f = 33\%$ machining is by discontinuous chip formation. During continuous chip formation, the cutting force asymptotes to a steady state value with increasing tool displacement. A typical chip is shown in Fig. 5(a), and at higher magnification in Fig. 5(b). A fine grid was scribed on the specimen in order to deduce the nature of the cutting process and this showed

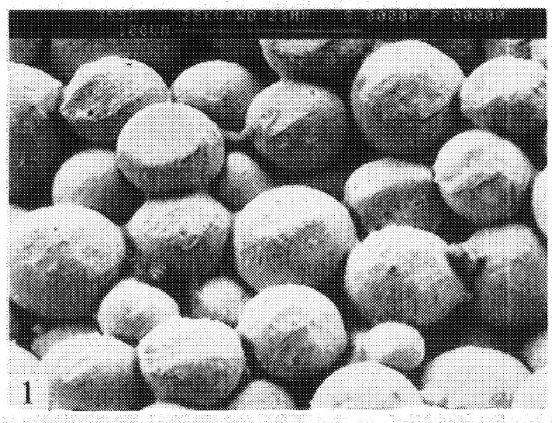

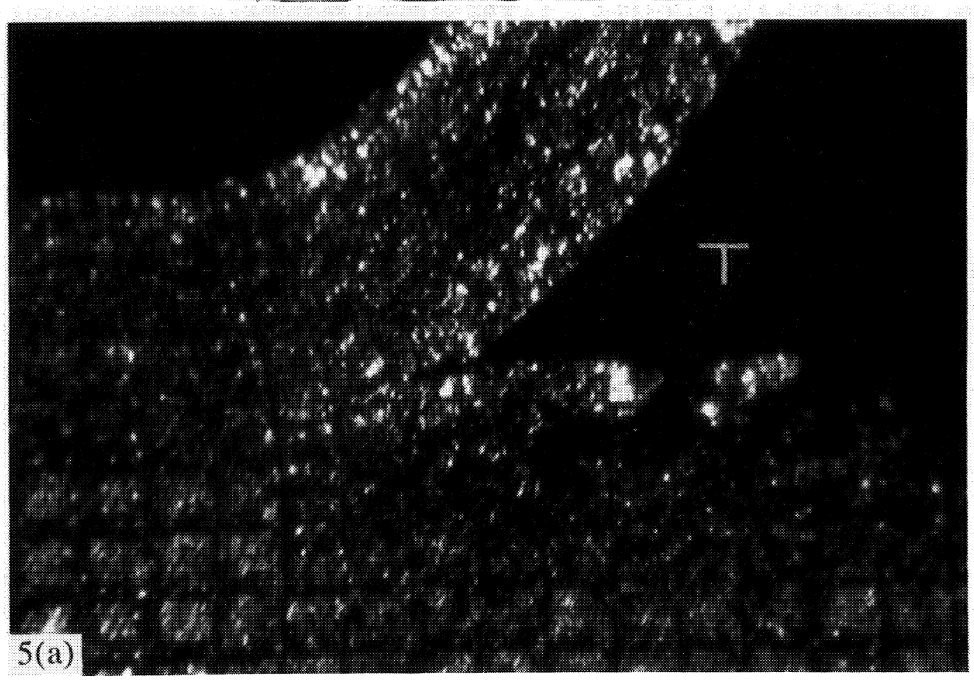

Fig. 1. A representative view of as-sintered porous bronze. Porosity $f = 40\%$.

Fig. 5. Continuous chip formation in 23% porous bronze and in copper, due to a tool with a 45° rake angle and no relief. (a) 23% porous bronze, (b) higher magnification view and polished surface of 11% porous bronze, (c) 1/2 hard copper. In all cases depth of cut = 0.5 mm. A 0.2 mm spacing grid was scribed prior to machining in order to show the deformation pattern. The capital letter T added to the micrographs denotes the location of the 45° tool; the machining direction is from right to left.

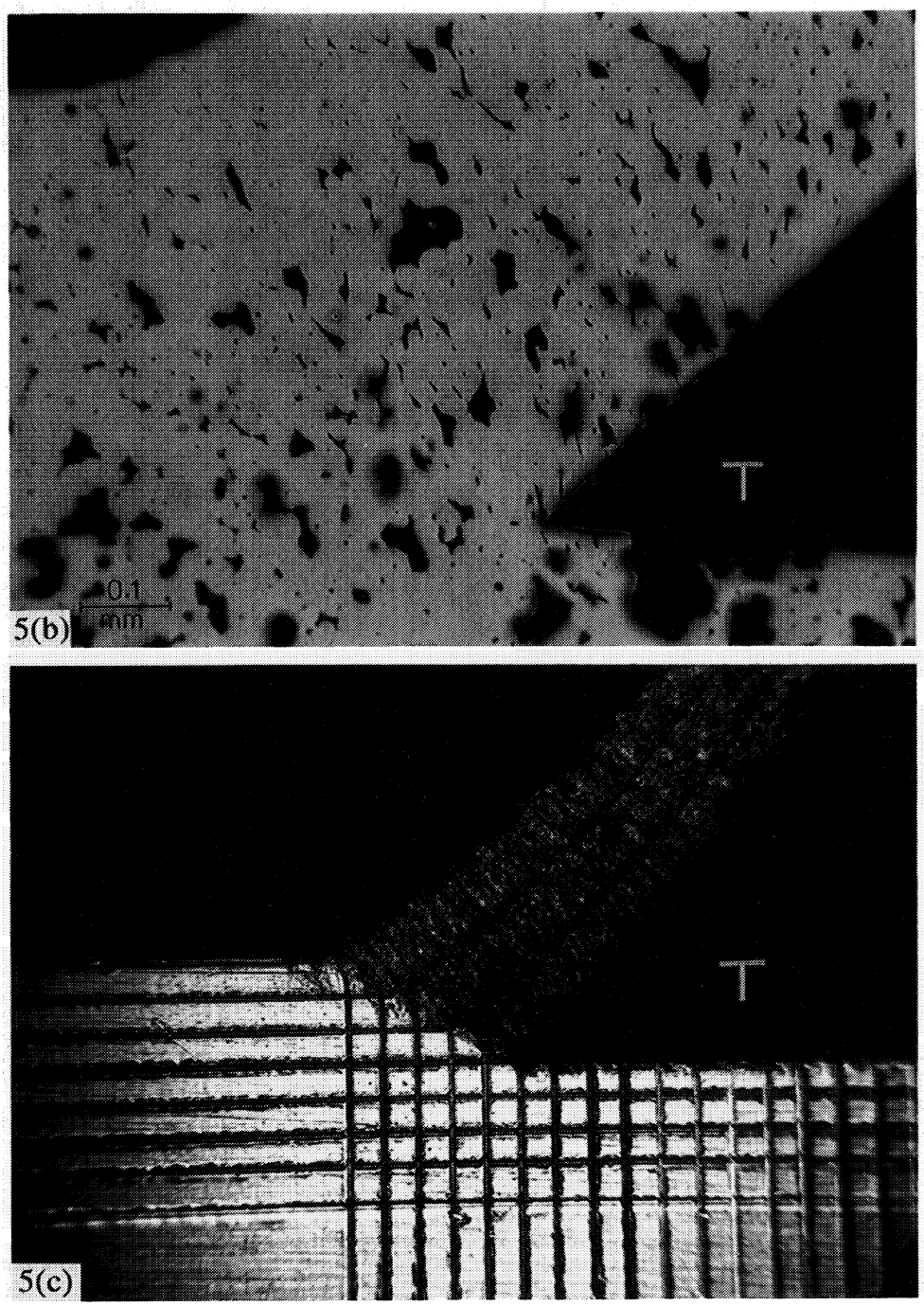

Fig. 5.(b, c) (*continued*)

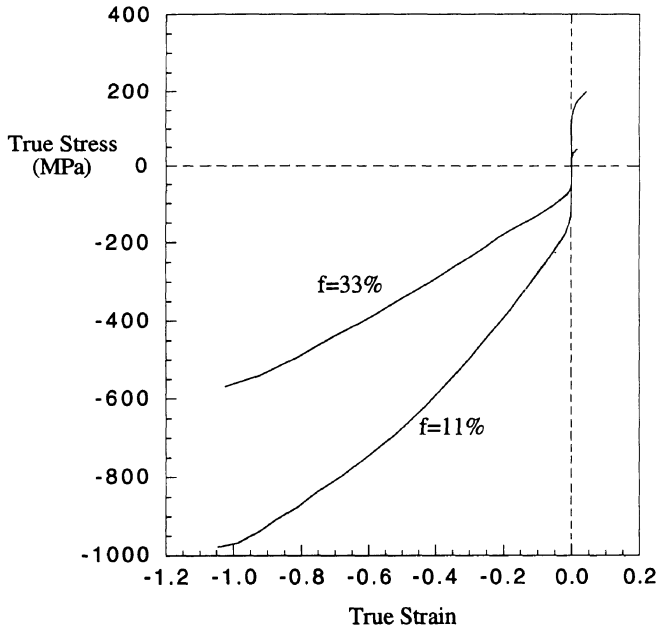

Fig. 2. Uniaxial true stress vs true (logarithmic) strain response for the sintered bronze, at $f = 12\%$ and $f = 33\%$. The 11% porous specimen failed in tension at a strain $\varepsilon = 5\%$, and the 33% porous specimen failed in tension at $\varepsilon = 2\%$. The specimens did not fail in compression.

Table 1. Preparation and properties of porous bronze specimens

Porosity, f	11%	23%	33%
Sintering temperature (1 h)	750°C	800°C	850°C
VHN	22.7	34.0	62.9
E (GPa)	80	–	19
σ_y (MPa)	142	87	34
K_{IC} (MPa$\sqrt{m}$)	15.6	8.9	1.5

that machining occurs by combined compaction and shear in a diffuse zone emanating from the tip of the tool. Typically, the porosity within the chip is half that of the undamaged specimen.

For comparison purposes a machining experiment was conducted on half-hard copper (yield stress = 250 MPa). Again, a grid was scribed on the specimens in order to elucidate the cutting mechanism. In this case, a narrow shear zone extends from the tool tip and gives rise to the continuous chip formation, see Fig. 5(c). The copper does not densify and strain hardens less than the porous bronze; consequently, plastic deformation is concentrated along an effectively concentrated shear plane.

3.2. *Discontinuous chip formation*

During discontinuous chip formation the cutting force F fluctuates with a more or less constant wavelength of about twice the depth of cut, d, see Fig. 4. In order to examine the details of chip formation, a test was interrupted at four stages of machining (labelled A–D) in Fig. 6(a), and the specimen was examined using a SEM; the resulting micrographs are given in Fig. 6(b). Consider a representative load cycle A–D as shown in Fig. 6(a). Prior to maximum load the chip undergoes compaction much in the manner of that described for

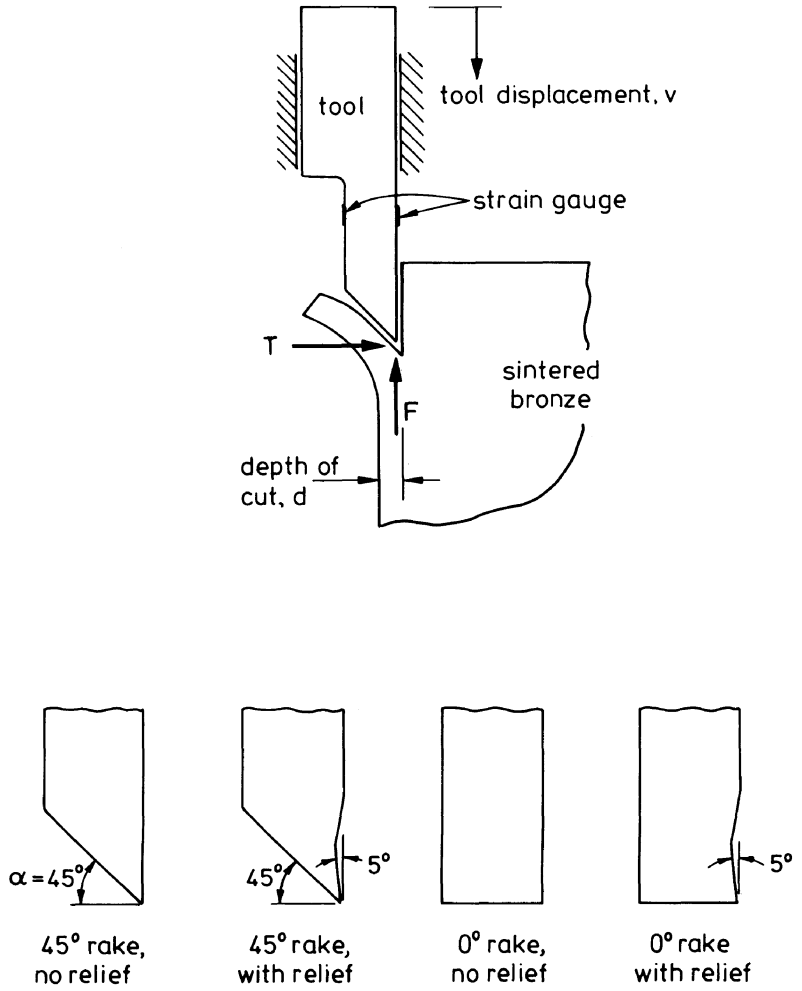

Fig. 3. Machining rig.

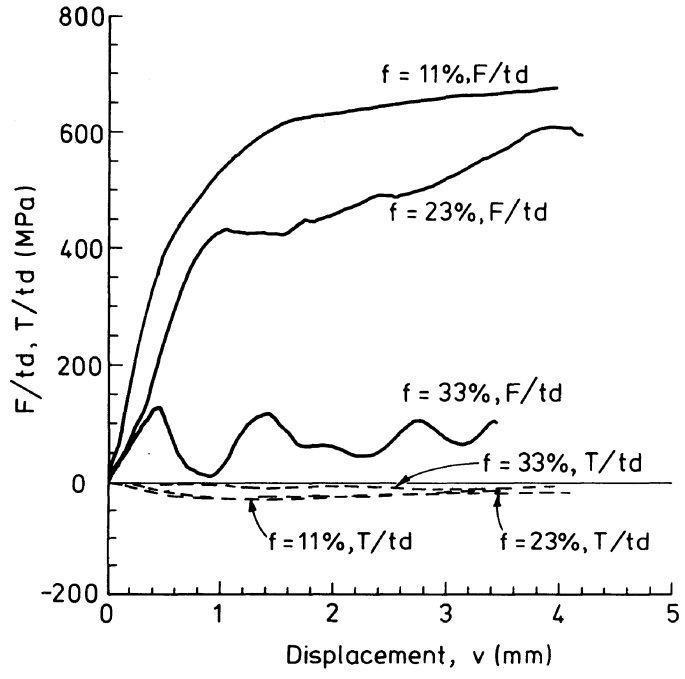

Fig. 4. Observed normal cutting pressure F/td and transverse cutting pressure T/td plotted against tool displacement v, for a cutting depth of 0.4 mm and porosities in the range 11%–33%.

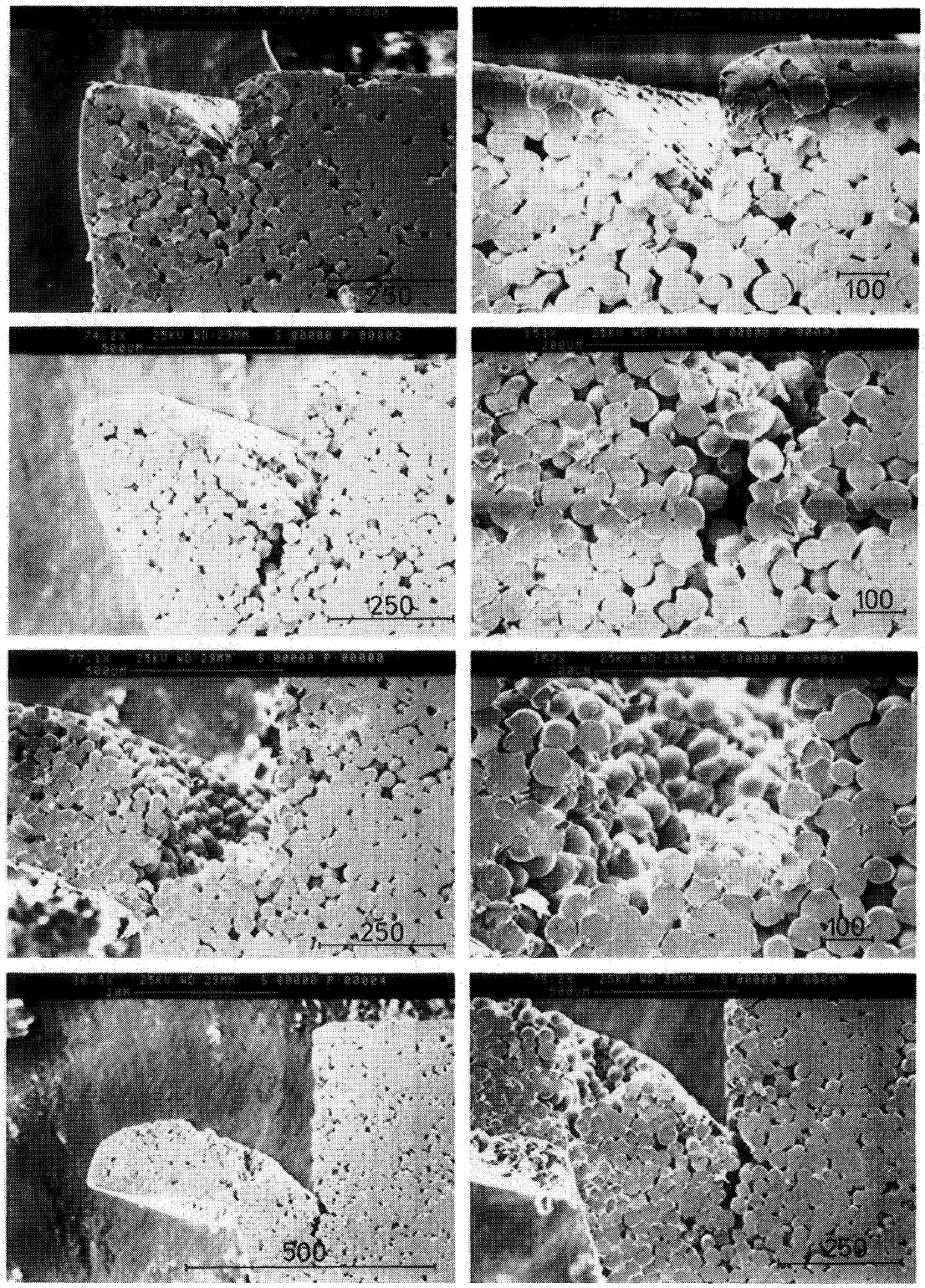

Fig. 6. Discontinuous chip formation in 33% porous bronze, depth of cut = 0.4 mm, tool has 45° rake angle with no relief. (a) Oscillation in cutting force with increasing tool displacement, (b) mechanism of cutting over a typical load cycle. The scale bars on the micrographs are in μm.

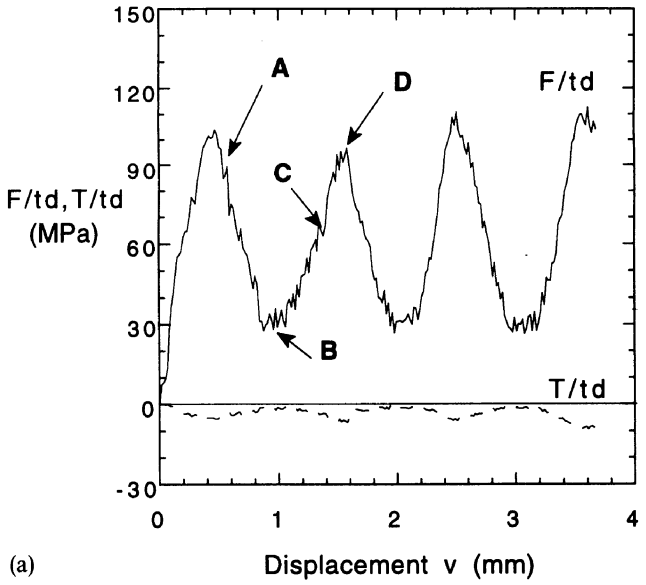

(a)

Fig. 6(a).

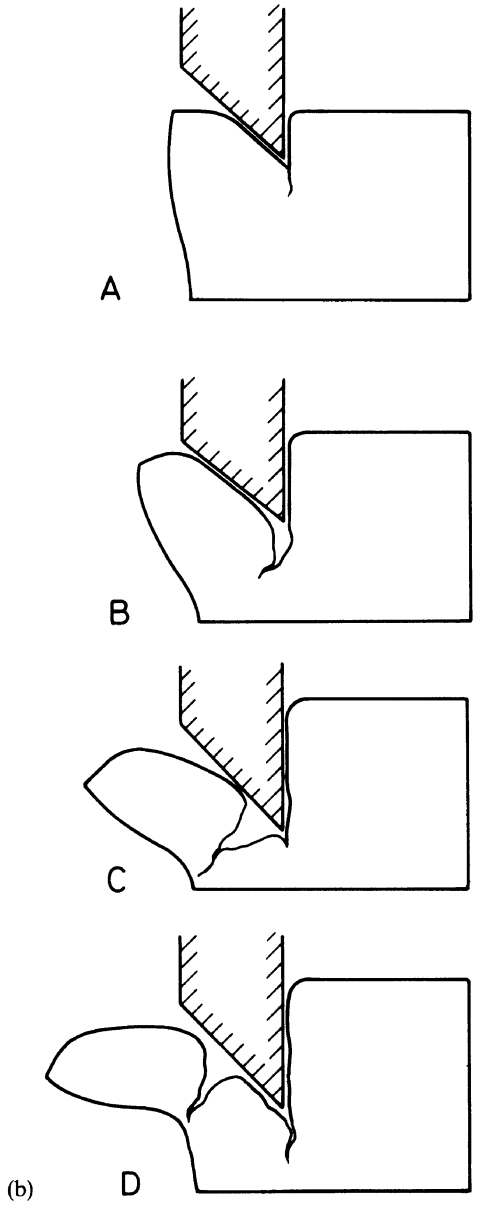

(b)

Fig. 6(b) (line outlay).

continuous chip formation. However, at loads close to maximum load, a brittle tensile, or mode I, crack develops from the tip of the tool and grows in a stable manner towards the free surface of the chip, stage B. At this stage the magnitude of the cutting force is set primarily by bending of the ligament of the chip. With increasing displacement of the tool, the tool compacts material beneath it and the cutting force F increases again, stage C. Finally, a new crack initiates at the tip of the tool and the process repeats itself, step D. This mechanism of discontinuous chip formation is similar to that described by Bannerjee and Palmer [1] and discussed further in Johnson and Mellor [2] for fully dense metals.

3.3. *Machining map*

The energy consumed in metal cutting can be ascribed to three mechanisms *viz* plastic work associated with the formation of the chip, frictional work principally at the interface between the chip and the rake face of the tool, and the work of fracture in separating the chip from the parent material or, perhaps, in subsequently fragmenting the chip. The conventional view of orthogonal machining is that the first two of these mechanisms are of greater importance and that intense shear occurs in a narrow band extending from the tip of the tool to the outer free surface. However, as Atkins [3] has pointed out, plasticity and fracture are not mutually exclusive and, indeed, the cyclical force characteristic observed in some of these experiments suggests that crack propagation is occurring during part of the cycle. A failure mechanism map may be constructed separating those conditions in which the work of fracture is significant from those in which plasticity is entirely dominant by taking porosity f and cutting depth d as axes. A suitable non-dimensionalization of the cutting depth is the group d/r_p where we take r_p to be the plane strain plastic zone size at onset of brittle fracture, i.e.

$$r_p = \frac{1}{3\pi}\left\{\frac{K_{IC}}{\sigma_y}\right\}^2 \tag{1}$$

where K_{IC} is the plane strain fracture toughness, as tabulated in Table 1.

The regimes of continuous chip formation and discontinuous chip formation are marked on to the map, for the case of a rake angle $\alpha = 45°$ and no tool relief, see Fig. 7. We observe continuous chip forms at low cutting depths. The transition to discontinuous chip formation occurs at $d/r_p = 0.6$ *independent of the level of porosity.* It appears that the role of porosity is subsumed within the non-dimensionalization for d.

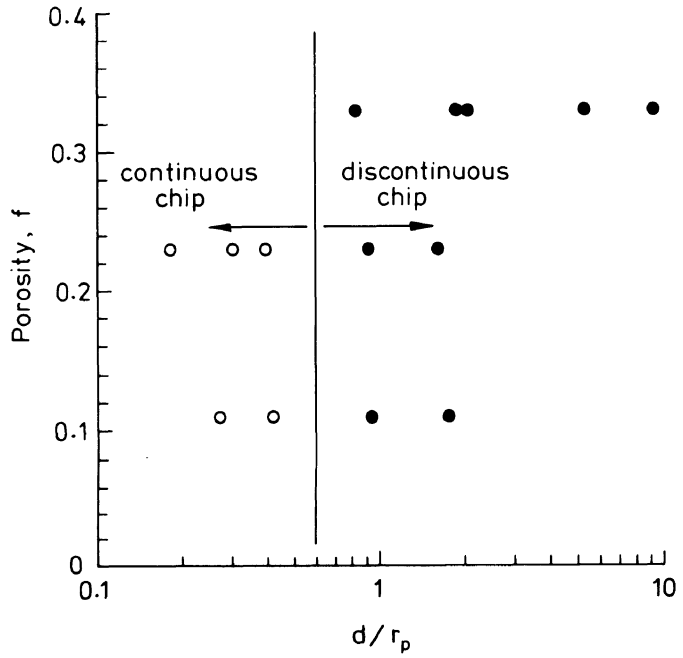

Fig. 7. Machining map for tool with a 45° rake angle and no relief. The axes are porosity f, and non-dimensional depth of cut. Regimes of continuous and discontinuous chip formation are delineated.

The ratio d/r_p has a straightforward physical interpretation. When $d \ll r_p$ chip formation occurs within a plastic field and machining is by a plasticity mechanism without the intervention of cracking. Consequently, a steady state is reached and the chip forms in a continuous manner. Alternatively, when $d \gg r_p$, the maximum machining load is limited by the growth of a crack from the tool tip. Material removal is by alternating compaction of material ahead of the tool tip and by brittle fracture: a discontinuous chip results.

During discontinuous chip formation the load F oscillates with increasing tool displacement, v, as shown in Figs 4 and 6(a). The wavelength λ increases in a roughly linear manner with depth of cut, such that $\lambda \approx 2d$, for all porosities considered, see Fig. 8.

3.4. *Effect of depth of cut on the machining load*

In orthogonal machining of fully dense solids the cutting pressure F/td is typically between 1 and 2 times the flow strength σ_f of the material, see for example the data in Oxley [4] and plasticity theories of machining predict no dependence of machining pressure upon depth of cut. The current results for continuous chip formation of the porous bronze are as summarized in Fig. 9(a). For a rake angle $\alpha = 0°$ the observed cutting pressure F/td is about 15 times the initial yield strength σ_y, and for a rake angle $\alpha = 45°$ we measured $F/td \approx 5\sigma_y$. It is thought that the high values of $F/td\sigma_y$ are due mainly to the fact that the sintered bronze strain hardens appreciably in compression. For $f = 11\%$ the flow stress in uniaxial compression increases from an initial value of $\sigma_y = 142$ MPa to one approaching 1000 MPa when the strain is increased from 0.1% to 100%.

Using the most straight-forward Merchant shear-plane model [5] of the orthogonal machining process, the cutting force F can be estimated from the equation

$$\frac{F}{tb\sigma_f} = \frac{2\cos(\tan^{-1}\mu - \alpha)}{1 - \sin(\tan^{-1}\mu - \alpha)} \tag{2}$$

where μ is the coefficient of friction on the tool rake face. If we set this to 0.4, a value not unreasonable for these conditions [1] then, when $\alpha = 0°$, $F/tb\sigma_f = 2.95$ and when $\alpha = 45°$, $F/tb\sigma_f = 1.32$. The ratio of the value of σ_f to σ_y is not known explicitly as it will depend on the detail strain history of the material within the deformation zone but examination of the deformation pattern of the scribed grid during continuous chip formation of the porous bronze shows that the material suffers large shear strains—typically approximately 0.7. This corresponds to a von Mises effective strain of more than 0.4 and we can note from Fig. 2 that, at uniaxial strains of this magnitude, the flow stress σ_f may easily be more than

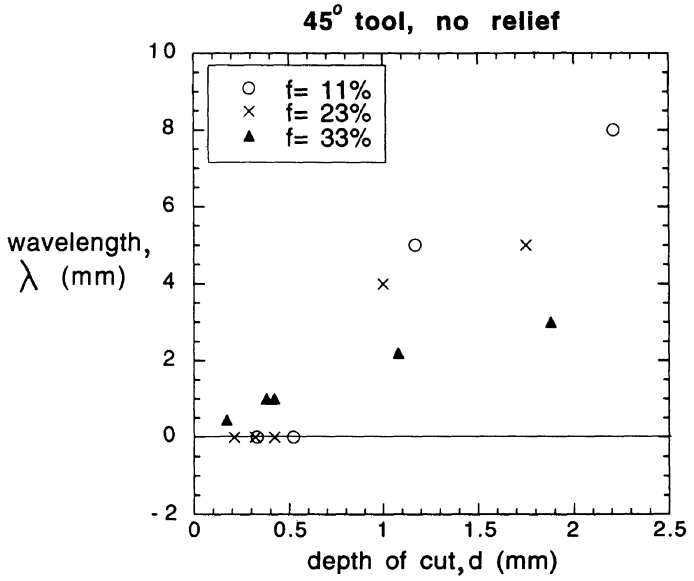

Fig. 8. Effect of depth of cut d upon wavelength λ (of cutting load vs tool displacement response). Tool has a 45° rake angle and no relief.

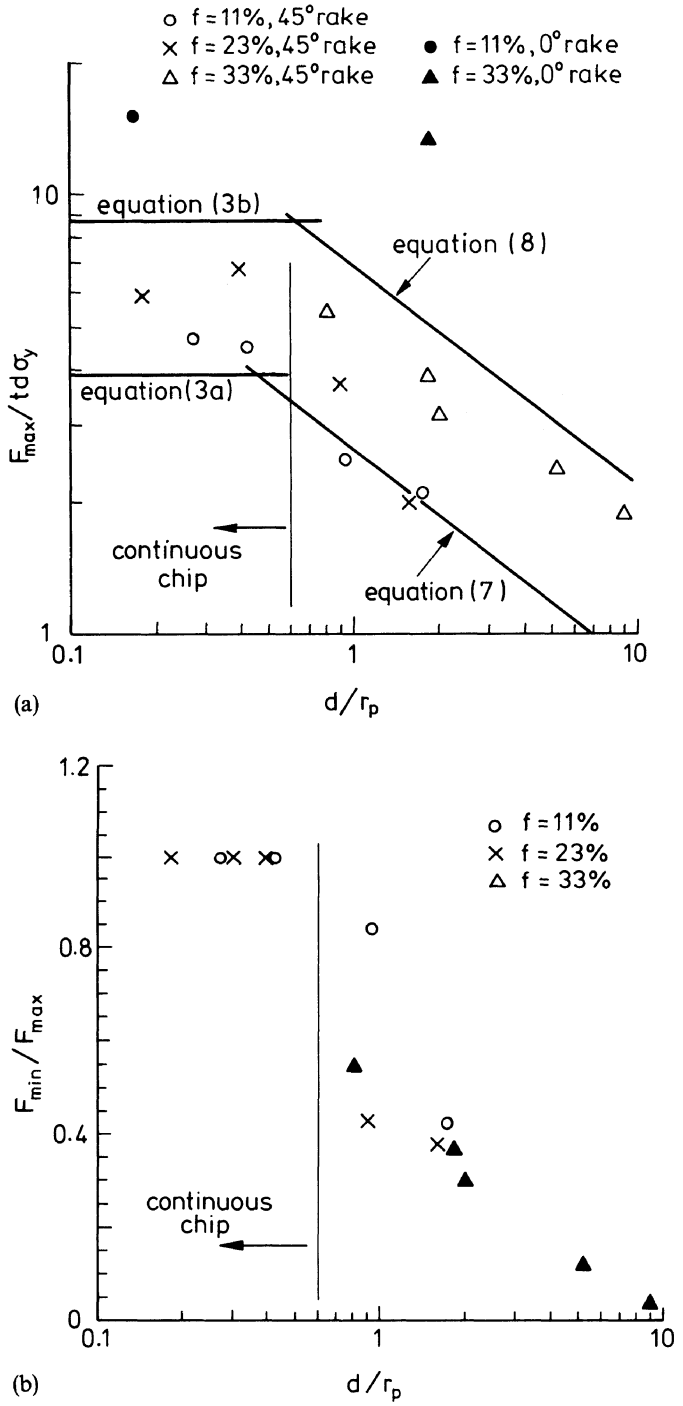

Fig. 9. Effect of cutting depth d upon (a) maximum cutting load and (b) magnitude of the oscillation in cutting load. Tool has a 45° rake angle and no relief.

3 times the value of the initial yield stress. Using this factor, the estimated values of the normalized force therefore become,

$$\frac{F}{tb\sigma_y} = 3.96 \quad \text{for } \alpha = 45° \tag{3a}$$

and

$$\frac{F}{tb\sigma_y} = 8.86 \quad \text{for } \alpha = 0°. \tag{3b}$$

These values are within a factor of 2 of those observed, see Fig. 9(a).

The maximum machining pressure during discontinuous chip formation decreases with increasing depth of cut, as shown in the non-dimensional plot of $F_{max}/td\sigma_y$ vs d/r_p in

Fig. 9(a). This suggests that the maximum load is set by the onset of brittle fracture from the tip of the tool. Theoretical support for this hypothesis is given in the following section. Following the attainment of maximum load tool advance is by the growth of a crack to the free surface. As the crack advances the load on the tool decreases as depicted in Fig. 6(a). The ratio of F_{min} to F_{max} during an oscillating load cycle decreases with increasing depth of cut as shown in Fig. 9(b).

3.5. *Crack advance during discontinuous chip formation*

The relation between the maximum cutting force attained during discontinuous chip formation and the depth of cut d can be estimated as follows. We assume elastic–brittle behaviour, and that the maximum load is associated with crack advance from the tip of the tool. Upon assuming the crack length l is much longer than the depth of the cut d we employ the K-calibration of Thouless *et al.* [6] for the crack geometry shown in Fig. 10. They consider a subsurface crack in a semi-infinite plate, under remote axial loading P per unit thickness and bending moment M per unit thickness. The complete solution is

$$K_I = 0.4347Pd^{-1/2} + 1.932Md^{-3/2} \tag{4}$$

and

$$K_{II} = 0.5577Pd^{-1/2} - 1.506Md^{-3/2}. \tag{5}$$

It is observed experimentally for the 45° tool that the crack advances directly ahead of the tool, i.e. parallel with the free surface, implying that $K_{II} \approx 0$, and thus from Eqns (4) and (5)

$$K_I \approx 1.150Pd^{-1/2}. \tag{6}$$

On identifying P with F/t and K_I with K_{IC} in the machining problem, the maximum load is estimated to be

$$\frac{F_{max}}{td\sigma_y} = 2.67\left(\frac{d}{r_p}\right)^{-1/2} \tag{7}$$

via Eqn (5). The prediction represented by Eqn (7) has been added to Fig. 9(a). Reasonable agreement is observed with the observed maximum cutting force considering the approximations involved.

The maximum cutting force has been added to Fig. 9(a) for the case of a 0° rake angle without relief of the flank face. Discontinuous chip formation was observed for the chosen value of depth of cut $d = 0.4$ mm. Note that the magnitude of the cutting force is about twice that observed for the 45° tool.

The cracking model may also be used to estimate the maximum load for the 0° tool. We assume that the imposed bending moment M on the chip is negligible, so that $K_I = 0.4347Pd^{-1/2}$ from Eqn (4). The non-dimensional cutting force is given by

$$\frac{F_{max}}{td\sigma_y} = 7.06\left(\frac{d}{r_p}\right)^{-1/2}. \tag{8}$$

Equation (5) shows that $K_{II} > 0$ at crack initiation and the crack kinks down into the bulk

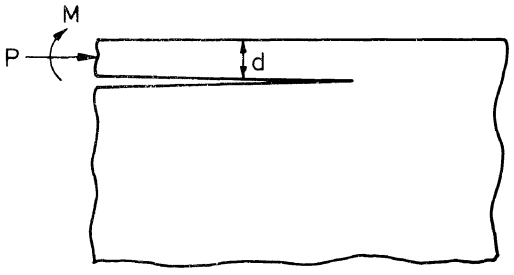

Fig. 10. Idealized geometry of an edge crack laying a distance d below the free surface of a semi-infinite solid, and subjected to remote axial load P per unit thickness and bending moment M per unit thickness.

of the solid. Observation confirms that the maximum load is set by this crack kinking step, after which the crack grows into the bulk extending along a curved path crack towards the free surface under a decreasing machining force. Comparison of Eqn (8) with the experimental data of Fig. 9(a) for the 0° tool shows acceptable agreement. It can also be noted that the intersections between Eqns (3a) and (7) and between (3b) and (8) representing respectively conditions with 45° and 0° tools both occur at values of the group d/r_p close to the experimentally observed value of 0.6.

3.6. *Effect of rake angle and tool relief on cutting mechanisms*

The effect of rake angle and relief of the flank face upon the machining force and wavelength of discontinuous chip is shown in Table 2, for a porosity of 11% and 33%. The cutting force as a function of tool displacement v is given in Fig. 11 for $f = 33\%$ and $d = 0.4$ mm. We observe no significant effect of tool relief on the machining process for both rake angles. For a given depth of cut, the cutting force is found to increase when the rake angle is increased from 45° to 0°. The wavelength of the load vs tool displacement response for the discontinuous chip is essentially independent of rake angle.

For the 0° rake angle transverse force T is about 1/4 of the cutting force F throughout the test. Tool relief has no significant effect on the transverse force. The transverse force is negative in sign, implying that the tool pushes the chip away from the parent material. This is surprising as friction over the rake face of the tool would give a positive value for the transverse force. Micrographic observations of the chip and the parent material show that the porous bronze compacts at the tip of the tool, and behaves as a built-up edge: this may be the underlying reason for large negative values for T.

Table 2. Cutting test results

Tool	45°, no relief		45° with relief		0°, no relief		0°, with relief	
Porosity, f	33%	11%	33%	11%	33%	11%	33%	11%
d (mm)	0.38	0.42	0.42	0.38	0.38	0.21	0.38	0.21
λ (mm)	1.0	0	1.1	0	0.9	0.75	3.0	1.0
$\frac{F_{max}}{td}$(MPa)	132	595	114	421	461	2140	500	2450

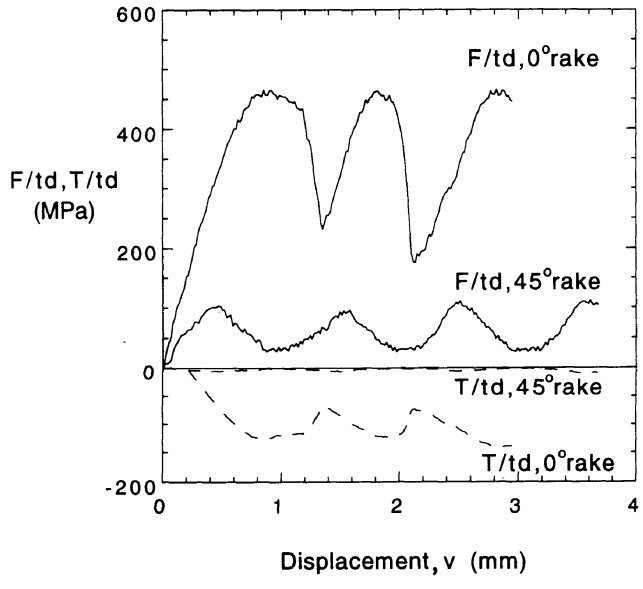

Fig. 11. Effect of rake angle upon cutting forces. For both the 45° and the 0° rake angles the tool has no flank relief. Porosity $f = 33\%$, and depth of cut $d = 0.4$ mm.

4. CONCLUDING DISCUSSION

In commercial machining practice it is important to maintain accuracy and surface finish. Stock removal by discontinuous chip formation is unacceptable, although it might be noted that chips *formed* continuously but subsequently broken up and fragmented by their passage over a chip breaker are desirable from the points of view of both handling and disposing of the swarf. For the porous bronze, continuous chip formation is achieved by keeping the depth of cut d less than the critical value d_{cr} given by the relation

$$d_{cr} = 0.6r_p = 0.064\{K_{IC}/\sigma_y\}^2. \tag{9}$$

When surface finish is unimportant (for example in material removal processes such as rock drilling) discontinuous chip formation has the advantage that it involves lower cutting forces.

Atkins [3] has examined discontinuous chip formation for a range of fully dense solids. He found that discontinuous chip formation begins at $d_{cr} = 0.6\{K_{IC}/\sigma_y\}^2$. The source of the discrepancy between Atkins's value of the critical depth of cut for mode transition and that of Eqn (9) can be ascribed to the large amount of strain hardening shown by the porous bronze, see Fig. 2 and referred to above. If the yield stress σ_y is replaced by this flow stress σ_f in our formula for the critical machining depth, i.e. Eqn (9), then discontinuous chip formation is expected at $d \approx 0.6\{K_{IC}/\sigma_y\}^2$, in broad agreement with the earlier work of Atkins.

Acknowledgements—The authors are grateful for helpful discussions with, and financial support from, Schlumberger Cambridge Research Ltd. Financial support for KJK also gratefully acknowledged via a KOSEF Fellowship.

REFERENCES

1. H. Bannerjee and W. B. Palmer, Metal cutting with a discontinuous chip. *Proc. 6th Int. M.T.D.R. Conf.* pp. 405–415. Pergamon Press (1966).
2. W. Johnson and P. B. Mellor, *Engineering Plasticity*. Van Nostrand Reinhold, New York (1973).
3. A. G. Atkins, Fracture toughness and cutting. *Int. J. Prod. Res.* **12**, 263–274 (1974).
4. P. L. B. Oxley, *The Mechanics of Machining*. Ellis-Horwood, Chichester (1989).
5. M. E. Merchant, Basic mechanics of the metal cutting process. *J. Appl. Mech.* **11A**, 168–175 (1944).
6. M. D. Thouless, A. G. Evans, M. F. Ashby and J. W. Hutchinson, The edge cracking and spalling of brittle plates. *Acta Metall.* **35**, 1333–1341 (1987).